Biosensors and Bioelectronics 126 (2019) 463–469

Contents lists available at ScienceDirect

Biosensors and Bioelectronics

journal homepage: www.elsevier.com/locate/bios

MoS_2/nitrogen doped graphene hydrogels p-n heterojunction: Efficient charge transfer property for highly sensitive and selective photoelectrochemical analysis of chloramphenicol

Ding Jiang[a,c], Xiaojiao Du[a], Qian Liu[a], Nan Hao[a], Kun Wang[a,b,*]

[a] School of Chemistry and Chemical Engineering, Jiangsu University, Zhenjiang 212013, PR China
[b] Key Laboratory of Sensor Analysis of Tumor Marker, Ministry of Education, College of Chemistry and Molecular Engineering, Qingdao University of Science and Technology, Qingdao 266042, PR China
[c] Department of Biomedical Engineering, The Hong Kong Polytechnic University, Hung Hom, Kowloon, Hong Kong, China

ARTICLE INFO

Keywords:
Chloramphenicol
Photoelectrohemical
MoS_2
Nitrogen doped graphene
p-n heterojunction

ABSTRACT

Constructing junctions between semiconductors is an effective way to promote charge separation and thus to improve the photoelectrochemical (PEC) performances, and specifically, p-n heterojunction is considered as a very promising structure. Herein, we designed and fabricated MoS_2/nitrogen doped graphene hydrogels (MoS_2/NGH) p-n heterojunction by a facile one-pot hydrothermal route. The as-fabricaterd MoS_2/NGH heterostructures demonstrated the excellent PEC activity, exhibiting enhanced photocurrent intensity by the fast transfer and separation rate of photogenerated electron-hole owing to the construction of p-n heterojunction. Based on the high PEC performances of the MoS_2/NGH heterostructure, a novel sensitive PEC sensor was developed for the determination of chloramphenicol (CAP) with the assistance of aptamer. In the presence of target molecules, the as-fabricated PEC sensor could recognize the CAP quickly and then consume the holes in the interface of heterostructures, inhibiting the recombination of photogenerated electron-hole pairs, resulting the enhanced photocurrent. Specially, with the concentration of CAP increased, the photocurrent enhanced gradually. Excellent linearity was obtained in the concentration range from 32.3 ng/L to 96.9 μg/L, and the limit of detection was 3.23 ng/L. Moreover, the as-fabricated PEC sensor exhibited rapid response, high stability, low-cost and high selectivity, which could be successfully applied to the analysis of CAP in honeycomb samples.

1. Introduction

Chloramphenicol (CAP) is a broad spectrum antimicrobial substance against infections caused by different types of micro-organisms (Liu et al., 2015; Miao et al., 2015). Owing to its low cost and efficient antibacterial effect, CAP has been widely used in food industry, livestock and poultry breeding industry (Wu et al., 2015). However, overusing of CAP as antibiotics and growth promoters will induce the accumulation in food-producing animals and diary food products such as milk, honey, meat and eggs, which may have some serious harmful effects on human beings, producing severe or fatal bone marrow, gray baby syndrome and cardiovascular collapse (Miao et al., 2015). Considering the toxic effects on humans, the CAP in food products is now strongly regulated by various organizations, and the minimum required performance limit (MRPL) for CAP in all foods of animal origin was set to be 0.3 μg/L by European Union (Unusan, 2009). Currently, various techniques have been employed to monitor the CAP, including gas chromatography-mass spectrometry (Posyniak et al., 2003), liquid chromatography-mass spectrometry (Rodziewicz and Zawadzka, 2008), chemiluminescence (Tao et al., 2013), and enzyme-linked immunosorbent assay (Impens et al., 2003). Although these methods fulfill the sensitivity requirement (MRPL), most of them have limitations in terms of the costs incurred by the expensive equipment and also require time-consuming operation procedures. Therefore, it is necessary and extremely important to develop a simple and fast method to sensitive and selective detection of trace CAP in food products.

Photoelectrochemical (PEC) sensing is a vibrantly developing analytical method, which shows great promise in bioanalysis, pollutant monitoring and medical diagnoses (Zhao et al., 2015). PEC detection technique utilizes light as the excitation source and the generated photocurrent as a detection signal, which is based on the relationship between the changes of photocurrent and the concentration of target analytes under light illumination (Zhao et al., 2017). Such efficient separation of stimulation source (optical signal) and detection signal

* Corresponding author at: School of Chemistry and Chemical Engineering, Jiangsu University, Zhenjiang 212013, PR China.
E-mail address: wangkun@ujs.edu.cn (K. Wang).

https://doi.org/10.1016/j.bios.2018.11.018
Received 20 September 2018; Received in revised form 8 November 2018; Accepted 13 November 2018
Available online 15 November 2018
0956-5663/

(electrical signal) provides a low background signal, leading to the high sensitivity and low detection limit (Zang et al., 2017; Hou et al., 2018). Morevoer, by coupling the photoirradiation with electrochemical system, PEC sensors integrate the advantages of both electrochemical sensors and optical methods, including easy operation, rapid measurement speed, miniaturization capability and inexpensive instrumentation (Zhao et al., 2016).

Generally, the typical PEC sensors necessitates photoactive materials as electrodes which can convert photoirradiation to electrical signal. Therefore, photoactive materials act as a crucial role for the performance of the PEC sensors. Of many photoactive materials aimed at producing high-efficient and low-cost optoelectronic devices, two-dimensional (2D) materials-based heterojunctions appear particularly promising for PEC applications, owing to their intriguing optical, electronic, and mechanical properties (Xu et al., 2016; Zhou et al., 2018). As a typical 2D transition metal chalcogenide (TMD) material with strong intralayer covalent bonding but weak interlayer van der Waals interaction, molybdenum disulfide (MoS_2) nanosheet exhibits excellent electrical and optical properties with unique direct bandgap features for a large number of optoelectronic applications (Shi et al., 2016; Xu et al., 2018; Jiang et al., 2017). In particular, nanostructured MoS_2-based heterostructures could generate the internal electric field at the contact surface, which may contribute to the photoinduced charge separation, inhibit the recombination rate, and increase the lifetime of charge carriers, thereby leading to enhancement in photoconversion efficiency and better performances in PEC applications (Liu et al., 2017; Li et al., 2017). Meanwhile, three-dimensional nitrogen doped graphene hydrogel (NGH) not only merits the excellent characteristics of nitrogen doped graphene including outstanding electrical conductivity, fast charge transfer ability and enhanced light harvesting (Jiang et al., 2016a, 2016b; Hou et al., 2013), but also has an exceptionally advantages of three dimensional macrostructures, which can support rapid electron transport in 3D space, promote efficient charge transfer and provide adequate space for molecular adsorption (D. Jiang et al., 2017; Y.Q. Jiang et al., 2017; Hao et al., 2017). Therefore, the coupling MoS_2 with NGH materials to construct nanocomposite may provide a new kind of photoactive material with fast transfer and separation rate of photogenerated electron-hole, which might have a high-performances in PEC sensing.

Herein, we report the PEC analysis of CAP in food samples by MoS_2/NGH heterojunctions with the assistance of CAP aptamer. As well-known aptamers possess high recognition ability to specific targets, and have the advantages of small size, good stability and easy modification, which are beneficial for the fabrication of PEC sensors (Ge et al., 2016a, 2016b; Hu et al., 2016). Notably, the heterostructures displayed the excellent PEC activity, exhibiting enhanced photocurrent intensity by the efficient charge transfer. The as-fabricated PEC sensor demonstrated good performance with high stability, rapid response, wide linear detection range and certain selectivity, and was used for determination of CAP in honeycomb samples.

2. Experimental

2.1. Reagents

L-cysteine, sodium molybdate ($Na_2MoO_4{\cdot}2H_2O$), chloamphenicol (CAP), gentamicin (GS), chlorotetracycline (CIP), thiamphenicol (TAP), chlortetracycline (TCT), and streptomycin (ME) were purchased from Aladdin Reagent Co., Ltd. (Shanghai, China. Graphene oxide (GO) nanosheets were prepared according to modified Hummers' method (Gilje et al., 2007). The CAP aptamer was obtained from Sangon Biotech Co., Ltd. (Shanghai, China) with the following sequence:

5′ − ACTTCAGTGAGTTGTCCCACGGTCGGCGAGTCGGTGGTAG − 3′.

0.05 M Tris–HCl buffer (pH = 7.4) containing 0.2 M KCl, 0.10 M NaCl, 5.0 mM $MgCl_2$ and 1.0 mM ethylene diamine tetraacetic acid (EDTA) was used as the The stock solution for CAP aptamer. Ultrapure water (18.2 MΩ, Millpore Co.) was used throughout this work.

2.2. Apparatus

The as-prepared samples were characterized by transmission electron microscopy (TEM, JEOL JSM-6700 transmission electron microscope), scanning electron microscopy (SEM, Hitachi S4800), X-ray diffraction spectroscopy (XRD, Bruker D8 diffractometer with Cu Kα radiation of 1.54 Å), X-Ray photoelectron spectroscopy (XPS, ESCALab MKII X-ray photo-electron spectrometer), Raman spectra (confocal Raman system RM2000) and the electrochemical impedance spectroscopy (EIS, Zennium electrochemical workstation). The PEC and electrochemical measurements were conducted on CHI 760E electrochemical workstation (CH Instruments). Indium tin oxide (ITO) electrode, Ag/AgCl electrode and platinum wire were used as working electrode, reference electrode and counter electrode, respectively. The PEC behaviors of different modified electrodes were investigated in 0.1 M phosphate buffer solution (PBS, pH = 7.4) at the applied potential of 0 V under light irradiation, and 500 W Xe lamp (Beijing Changtuo Co., Ltd.) with a 400-nm cut-off filter was served as the light source.

2.3. Synthesis of MoS_2/NGH hydrogels

MoS_2/NGH hydrogels were prepared by a facile hydrothermal approach. Typically, 1 mM $Na_2MoO_4{\cdot}2H_2O$ was dissolved into 75 mL water, and then adjusted to pH 6.5 by HCl. After that, 0.5 g L-cysteine and different amounts of GO solutions were mixed with above solution, and then transferred into a 100 mL Teflon-lined stainless steel autoclave and maintained at 200 °C for 36 h. After it cooled down naturally, the black products could be taken out directly and washed with water for several times. Finally, MoS_2/NGH hydrogels with different amounts of NGH were obtained by freeze-drying. For comparison, the NGH hydrogels were prepared using the same process without the addition of $Na_2MoO_4{\cdot}2H_2O$. And MoS_2 nanoplates were synthesized through the same hydrothermal method without GO.

2.4. Preparation of the samples modified electrodes

To prepare the MoS_2/NGH hydrogels modified indium tin oxide (ITO) electrodes, the MoS_2/NGH hydrogels suspension were obtained by dispersing 5.0 mg of the as-prepared nanocomposites in 2.5 mL of ultrapure water with ultrasonic agitation for about several minutes. Then the suspensions (40 μL) were coated on the ITO substrate with a fixed area of 0.5 cm^{-2}, and dried at 60 °C for 10 h. For comparison, TiO_2/NGR nanocomposites modified ITO electrodes were obtained following the same procedure.

Before modification, the indium tin oxide (ITO) electrodes were boiling for 0.5 h in 0.1 M NaOH, and then sonicated in water and alcohol for cleaning, respectively. To prepare the MoS_2/NGH hydrogels modified ITO electrodes, the MoS_2/NGH hydrogels suspension were obtained by dispersing 5.0 mg of the as-prepared nanocomposites in 2.5 mL of ultrapure water with ultrasonic agitation for about several minutes. Then 20 μL of MoS_2/NGH hydrogels suspension were coated on the ITO substrate with a fixed area of 0.5 cm^{-2}, and dried at 60 °C for 10 h to obtain MoS_2/NGH hydrogels modified ITO electrodes (MoS_2/NGH/ITO). As comparison, NGH/ITO and MoS_2/ITO were prepared following the same procedure.

2.5. Construction of the PEC aptasensor

20 μL of the CAP aptamer (4 μM) was dropped on the surface of the obtained MoS_2/NGH/ITO electrode. To make ensure the effective

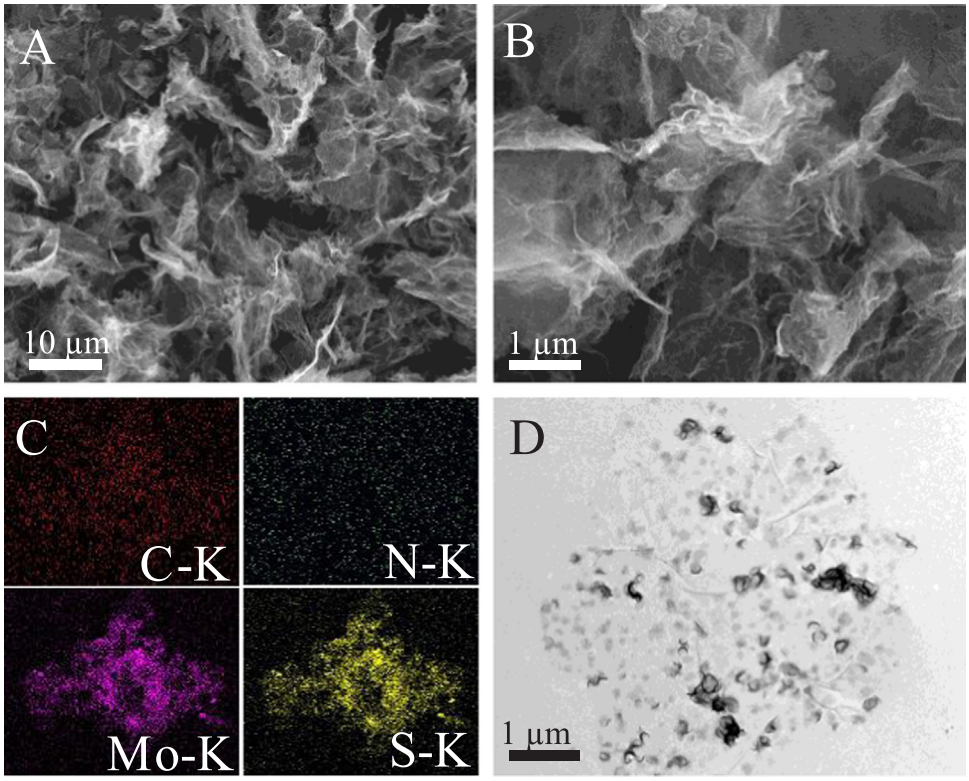

Fig. 1. (A, B) SEM images of MoS_2/NGH hydrogels. (C) Elemental distribution mapping of MoS_2/NGH hydrogels. (D) TEM images of MoS_2/NGH hydrogels.

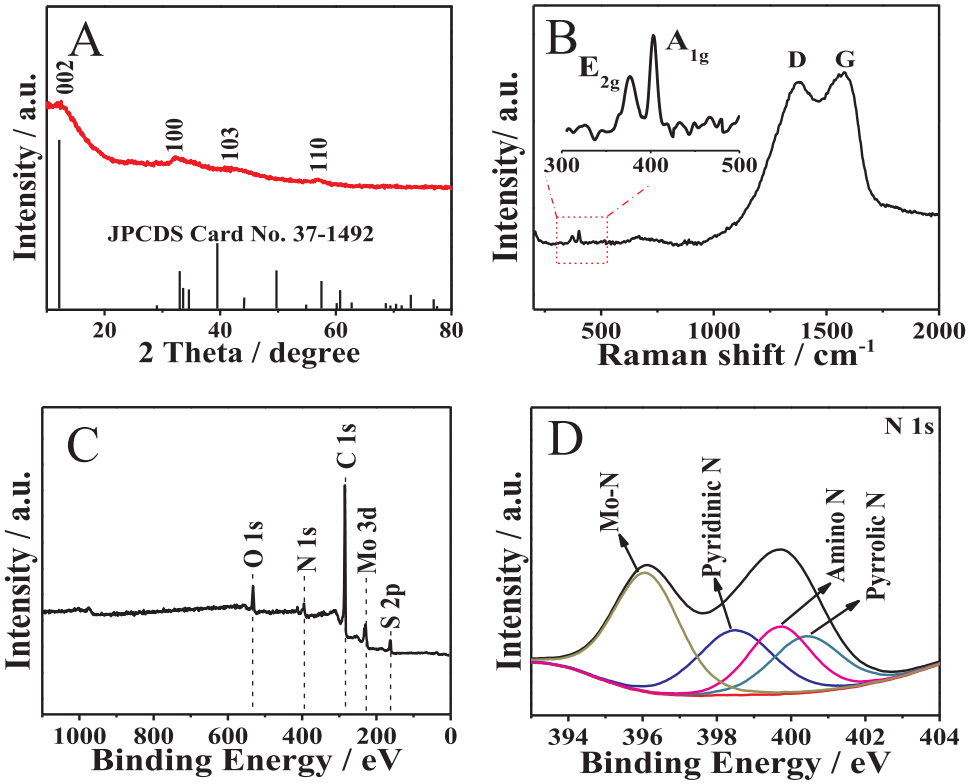

Fig. 2. XRD patterns (A), Raman spectra (B) and XPS survey spectra (C) of the MoS_2/NGH hydrogels. (D) The high resolution XPS of the N 1 s region for MoS_2/NGH hydrogels.

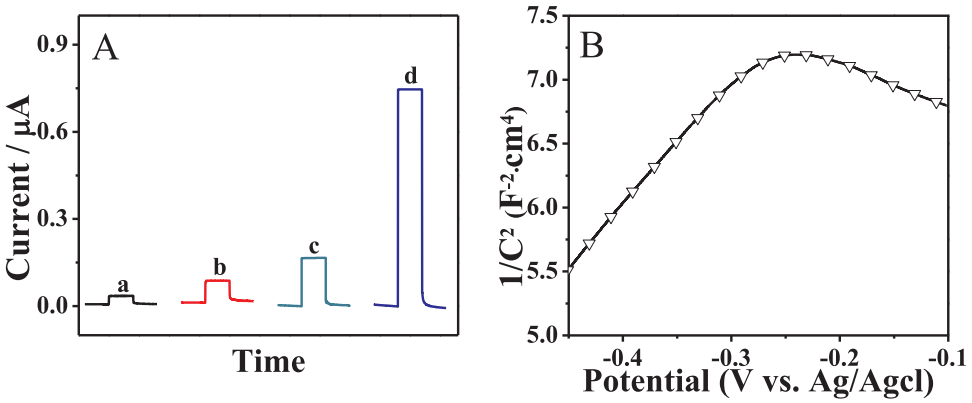

Fig. 3. (A) Photocurrent responses of ITO (a), MoS_2 (b), NGH (c) and MoS_2/NGH (d) modified ITO at a bias potential of 0 V. (B) The Mott-Schottky measurement of MoS_2/NGH hydrogels.

immobilization of aptamer, the electrode was placed at room temperature for 12 h. And then, the above electrode was washed by 0.1 M buffer solution to remove the excess non-adsorbed aptamer. For PEC sensing, 20 μL targets solutions with different concentrations were incubated on the ITO electrodes for some time and then washed through 0.1 M buffer solution for PEC measuring.

2.6. Sample preparation

1 g sample of honeycomb (from local market) was cut into very small pieces and was transferred to a flask containing 20.0 mL ethanol. After vigorously shaking and ultrasonication for 40 min, the mixture was centrifuged and the supernatant was collected for analysis.

3. Results and discussion

3.1. Characterization of the as-prepared MoS_2/NGH hydrogels

The morphology and microstructure of samples were measured by SEM and TEM. Fig. 1A and B showed the SEM images of the monolithic 3D MoS_2/NGH hydrogels. It is obvious that the as-synthesized MoS_2/NGH exhibited 3D porous network architecture with thin interconnected sheets. The hybrid aerogel maintains the porous features of the bare NGH, as seen in Fig. 1A and B. The open porous networks of the MoS_2/NGH allowed the aerogel surface area to be readily accessed and might facilitates charge transfer (Long et al., 2016; Hou et al., 2014). Elemental mapping images of C, N, Mo, and S elements for the MoS_2/NGH hydrogels were shown in Fig. 1C, which confirmed the uniform distribution of MoS_2 and NGH in the whole 3D architecture. The general morphology and microstructure of the MoS/NGH hydrogels were further investigated by TEM. As shown in Fig. 1D, the transparent NGH sheets with some folds were clearly observed. Moreover, the small laminar structured MoS_2 nanosheets were tightly dispersed on the surface of NGH sheets, forming the MoS_2/NGH heterostructure. Such interconnected network could increase the interfacial contact, and then promote the electrochemical performance (Lingappan and Kang, 2016).

XRD measurements has been performed to explore the crystal structure of the as-prepared MoS_2/NGH hydrogels. As shown in Fig. 2A, the peaks at 14.3°, 33.8°, 39.6° and 57.5° can be indexed as the (002), (100), (103) and (110) plane of the hexagonal MoS_2 phase, respectively (JCPDS 73-1508) (Jaiswal et al., 2017; Chao et al., 2017). The high intensity of (002) peak means stacked layered structure of MoS_2 crystals, which were corresponding to a *d*-spacing of 0.62 nm (Huang et al., 2015). However, there was no diffraction signal of NGH can be found, which probably resulted from the relatively low diffraction intensity of NGH. Further structural and electronic properties were obtained by Raman spectroscopy (Fig. 2B). The spectra exhibited two strong peaks at 1332 and 1594 cm^{-1}, which were matched well with the D and G bands of the graphene-based structure, respectively (Long et al., 2016; Chao et al., 2017). Furthermore, the inset figure ranging from 300 to 500 cm^{-1}, displayed two major peaks A_{1g} (382 cm^{-1}) and E^1_{2g} (408 nm^{-1}). The A_{1g} peak is corresponded the out-of-plane vibration of two S atoms in the opposite directions, while the E^1_{2g} peak were derived from the symmetric vibration of S atoms opposite to Mo atom within the S-Mo-S layer (Jaiswal et al., 2017; Chao et al., 2017). All these data showed the characteristic peaks of MoS_2 and graphene, indicating the MoS_2/NGH hydrogels were prepared successfully.

The surface chemical compositions and chemical states of MoS_2/NGH were further analyzed by using XPS. As can be seen from Fig. 2C, the survey scan spectrum showed that C, N, Mo, S and O were clearly identified in the as-synthesized MoS_2/NGH hydrogels. The high-resolution scans of Mo 3d and S 2p were shown in Fig. S1. As shown in Fig. S1A, there were two strong peaks (229.1 eV and 232.5 eV) could be observed, corresponding to Mo $3d_{5/2}$ and Mo $3d_{3/2}$, respectively. These values are characteristic of Mo^{4+} species in the form of pure MoS_2 (Long et al., 2016). Furthermore, a small peak locating at 235.6 eV indicated the presence of Mo^{6+}, which could be attributed to the slight oxidation on the surface of MoS_2 edges (Hou et al., 2014; Toth et al., 2016). The high-resolution spectrum of S 2p (Fig. S1B) displayed two characteristic peaks (S $2p_{3/2}$ at 161.9 eV and S $2p_{3/2}$ at 163.2 eV), indicating the formation of MoS_2 (Toth et al., 2016). The high-resolution N spectrum in MoS_2/NGH is shown in Fig. 2D, and the broad peak could be deconvoluted into four peaks. The peaks located at 398.4, 399.7 and 400.4 eV, could be assigned to the pyridine nitrogen, amine nitrogen and pyrrolic nitrogen in the nanocomposites (Jiang et al., 2014). Notably, the peak at about 396.1 eV indicated the formation of Mo-N bond, which could increase the interfacial contact between MoS_2 and NGH, and then promote the charge transport of the overall heterostructure (Lingappan and Kang, 2016).

3.2. Characterizations of the as-prepared samples modified electrodes

The photoelectronic response of different samples modified electrodes were studied by acquiring the transient photocurrent responses in the different light switching states. As we can see in Fig. 3A, the bare ITO (curve a) displayed a very small photocurrent. Meanwhile, the pristine NGH (curve b) and pure MoS_2 (curve c) modified ITO electrode exhibited a weak photocurrent of 0.143 μA and 0.224 μA, respectively. After NGH was introduced to the MoS_2, the MoS_2/NGH nanocomposites modified ITO electrode (curve d) dispalyed much enhanced photocurrent (0.756 μA), which was about 5.3 times and 3.4 times than that of NGH and MoS_2, respectively. The obviously enhanced photocurrent intensity of MoS_2/NGH revealed the positive effect of NGH on facilitating the generation and separation efficiency of photoexcited charge carriers of MoS_2. Moreover, a high surface-to-volume ratio of the three-dimensional hierarchical heterojunction materials might have favorable

effects for photoactive performance (Chang et al., 2014).

The interfacial charge transfer of MoS_2 and NGH modified electrodes were investigated by electrochemical impedance spectra (EIS). It is well known that the smaller arc radium of Nyquist plot means faster interfacial charge transfer and more effective separation of the electron-hole pairs (Jiang et al., 2016a, 2016b). As can be seen in Fig. S2, MoS_2/NGH nanocomposites (curve d) exhibited smaller semicircle compared with pure MoS_2 (curve c) and NGH (curve b), which further demonstrated that the hybridization of NGH with MoS_2 could be greatly beneficial to the efficient charge transfer. This phenomenon might be attributed to three reasons: 1) the high charge mobility of NGH which could fast transfer the charge carries to electrode. 2) the porous 3D structure of the nanocomposites which could effective stimulate the electron transport between NGH and MoS_2. 3) the formation of interfacial electric field between p-MoS_2 and n-NGH, resulting faster interfacial charge transfer and more effective separation of electron-hole pairs (Jiang et al.,2016a, 2016b, 2018). In order to further prove the formation of the p-n junction in MoS_2/NGH nanocomposites, Mott-Schottky measurement was measured in 0.5 M Na_2SO_4. As shown in Fig. 3B, the MoS_2/NGH heterostructured composites exhibited an apparent reversed "V-shaped", which was the characteristic of p-n heterojunction. Similar to previous studies, such p-n heterojunction could drive the photoexcited electrons to the CB (conduction band) of n-type NGH whereas the holes migrate to VB (valence band) of p-type MoS_2, resulting in longer lifetime of photocarriers and efficient spatial charge separation, which is regarded as the most important reason for enhanced photocurrent signal (Carraro et al., 2015; Meng et al., 2013).

3.3. Characterization of the PEC aptasensor

The PEC sensor was then fabricated based on the excellent PEC performances of MoS_2/NGH nanocomposites with the assistance of CAP aptamer as shown in Fig. 4A. With the presence of target, the CAP could specific bind to its aptamer, and then the photocurrent response increased owing to the photocatalytic reactions of CAP molecules captured by aptamer on the electrode surface (Jodat and Jodat, 2014; Lin et al., 2016; Liu et al., 2016; Hu et al., 2018; Tian et al., 2018). Similar to previous studies, the photogenerated holes on electrode surface could directly oxidize CAP molecules, or react with OH^- or H_2O to form $OH^{\bullet}$ radicals, and then oxidize CAP molecules, which inhibited the recombination of photogenerated electron-hole pairs, resulting the increase of a high photocurrent. Moreover, the photocurrent signal increased gradually with the increase of CAP concentration. As a result, the quantitative detection of CAP was acquired by monitoring the photocurrent signal.

EIS was performed to measure the interface properties variation of the stepwise assembly process of the PEC aptasensor by using $[Fe(CN)_6]^{3-/4-}$ as a redox probe. As exhibited in Fig. 4B, because of the low conductivity of ITO, the bare ITO electrode displayed a relatively high electron-transfer resistance (curve a, $R_{et} \approx 173\,\Omega$). After the MoS_2/NGH hydrogels were dropped on the surface of ITO, the R_{et} value decreased greatly (curve b, $R_{et} \approx 72\,\Omega$), suggesting higher efficiency of charge separation and faster interfacial charge transfer occurred in the MoS_2/NGH hydrogels. However, after the immobilization of aptamer on the modified ITO electrode, the CAP aptamer was bonded in the NGH through π-π stacking and the R_{et} increased to 89 Ω (curve c). The reason might be attributed to the negative aptamer molecules induce the electrostatic repulsion between the electrode surface and the negatively charged redox species of $[Fe(CN)_6]^{3-/4-}$ (Jiang et al., 2016a, 2016b; Liu et al., 2016). These results verified the successful modification of the CAP aptamer on the MoS_2/NGH/ITO electrode.

Fig. 4C further displayed the PEC characterization of the aptasensor fabrication process. After the immobilization of MoS_2/NGH hydrogels on the electrode, the photocurrent signal (0.78 μA, curve b) increased greatly than that of bare ITO electrode (0.03 μA, curve a), which might be ascribed to the enhanced lifetime of photocarriers and efficient spatial charge separation. Subsequently, the photocurrent signal decreased to 0,47 μA (curve c) after the modification of low conductivity CAP aptamer. However, in the case of CAP specific binding with aptamer/MoS_2/NGH/ITO electrode, the photocurrent increased

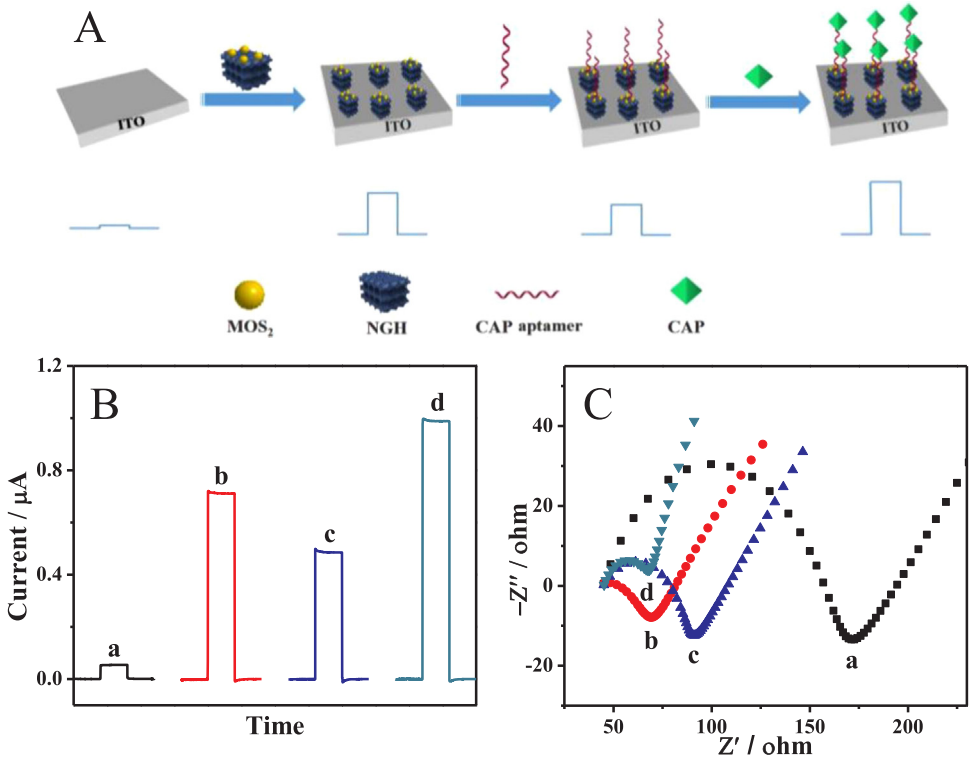

Fig. 4. (A) Scheme of the stepwise assembly process for the PEC aptasensor. (B) EIS spectra and (C) Photocurrent responses of a bare ITO (a); MoS_2/NGH (b), aptamer/MoS_2/NGH (c), CAP/aptamer/MoS_2/NGH (d) modified ITO at a bias potential of 0 V.

obviously (1.02 μA, curve d). The increased photocurrent response could be attributed to the photocatalytic reactions of CAP molecules captured by aptamer on the electrode surface. All these results above proved the successful stepwise assembly process of each sensing unit.

3.4. Optimization of experimental conditions

Obviously, the contents of NGH in MoS_2/NGH hydrogels could have an effect on the photocurrent signal. As shown in Fig. S3A, the photocurrent signal increased greatly with the contents of NGH increased from 0% to 30%, then the photocurrent was declined when the contents of NGH continued to increase. Such phenomenon suggested that 30% NGH in MoS_2/NGH hydrogels could be able to provide more photogenerated hole-electron pairs to participate in the PEC process. Thus, the optimal content of NGH in MoS_2/NGH hydrogels was 30%, which was chosen in the following experiments. The influence of the aptamer concentration on the sensing performance was further measured by the difference of photocurrent before and after incubation with CAP ($\otimes I$). As illustrated in Fig. S3B, the PEC response increased gradually with the increasing concentration of CAP aptamer from 0.5 μM to 4 μM, and then nearly reached a plateau. Therefore, 4 μM CAP aptamer was selected for fabricating the sensor. Furthermore, the performance of this aptasensor could also be affected by the incubation time between CAP molecules and aptamer. As can be seen in Fig. S3C, in the rang of 0 min through 30 min, the photocurrent signal increased obviously with the incubation time increased, and then reached a maximum value in 30 min. Consequently, 30 min was selected as the optimal reaction time to efficiently facilitate the PEC assay.

3.5. PEC sensing of CAP

Under optimal experimental conditions, the developed aptamer/MoS_2/NGH/ITO electrode was employed to sensitive detection of CAP molecules. Fig. 5A and B displayed the PEC responses of aptamer/MoS_2/NGH/ITO electrode to different concentrations of CAP molecules. It is obvious that the photocurrent signal increased gradually as the concentrations of CAP increased, showing that more captured CAP molecules participated in the photocatalysis process. Moreover, the steady-state photocurrent in the presence of CAP might imply the binding/dissociation of the analyte to sustain the current. Moreover, there was a linear relationship between the concentrations of CAP and ΔI ($\Delta I = I - I_0$) in the range from 32.3 ng/L ~ 96.9 μg/L with the correlation coefficient of 0.998, while the I and I_0 represented the photocurrent signal of the aptamer/MoS_2/NGH/ITO electrode in the presence and absence of CAP, respectively. And the detection limit was estimated to be 32.3 ng/L (S/N = 3), which is much lower than those works in the Table S1. Such a high-performance PEC sensor can not only be useful for the rapid assay of CAP in water and food, but also can be satisfactory for detection of CAP in biological fluids and pharmaceutical formulations.

3.6. Selectivity and stability

To assess the specificity of the aptamer-based PEC sensor for CAP, The influences of other antibiotics (such as TAP, TCT, ME, GS) on the photocurrent signal of the fabricated PEC sensor were examined. It can be seen from Fig. 5C that none of these interferents could cause obvious changes in the photocurrent, while a significant photocurrent change was observed for the CAP. These results clearly demonstrated that the designed sensor has good selectivity for the detection of CAP. Furthermore, the stability is also important to evaluate the practicability of the sensor. In this work, the stability was investigated by measuring its photocurrent signal over 20 days. As shown in Fig. 5D, the photocurrent signal of the as-fabricated sensor still remained about 88.9% even after 20 days, indicating that the PEC aptasensor displayed very stable performances. Moreover, five measurements for a single electrode were obtained upon the addition of 64.6 μg/L CAP in 0.1 M PBS with RSD of 5.7%, demonstrating the excellent reproducibility of the PEC sensor.

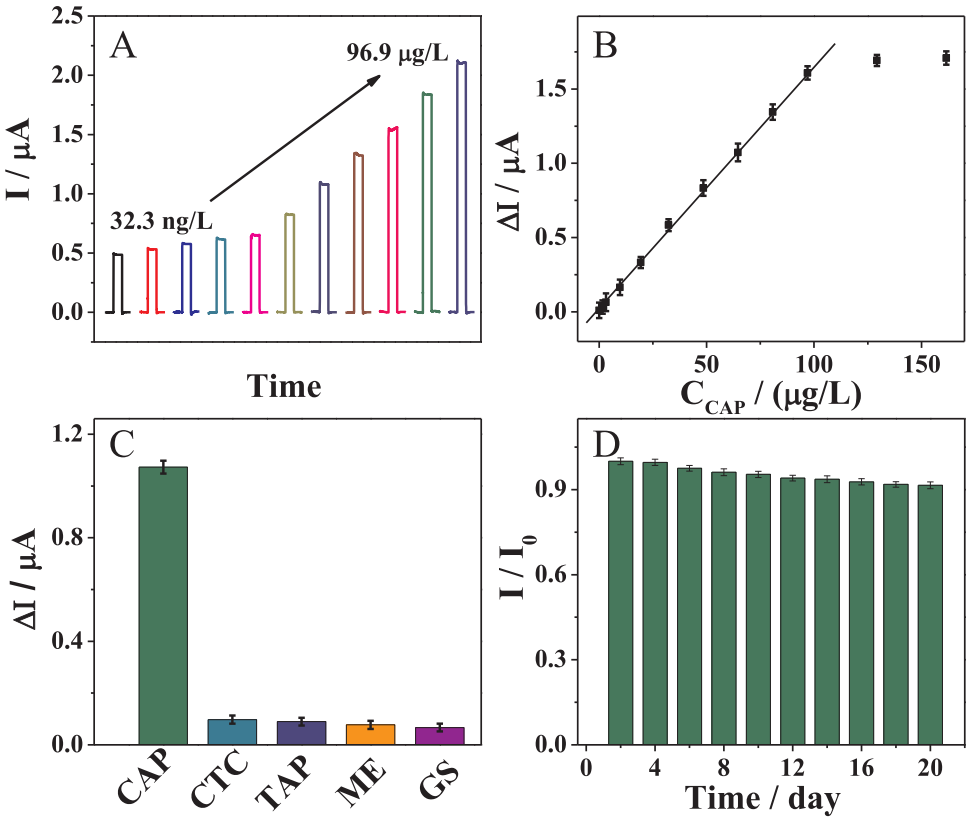

Fig. 5. (A) Effect of different concentrations of CAP on the photocurrent intensity of the aptamer/MoS_2/NGH/ITO electrode (from 0 to 96.9 μg/L), (B) Plot of photocurrent of the aptamer/MoS_2/NGH/ITO electrodeversus C_{CAP}, and the detection limit as low as 3.23 ng/L. (C) The selectivity of the as-fabricated PEC sensor with 64.6 μg/L CAP and 100 times higher amount of interfering compounds such as CTC, TAP, ME and GS. (D) The stability of the as-fabricated PEC sensor.

Table 1
Determination of CAP in honeycomb samples.

Sample	Added (μg/L)	Detected (μg/L)	Recovery (%)	RSD (%, n = 5)
1	32.31×10^{-3}	31.68×10^{-3}	98.1	4.3
2	1.62	1.72	106.2	3.9
3	9.69	10.15	104.7	5.7

Each sample was measured for five times.

3.7. Real sample analysis

The recoveries of CAP with different concentrations in honey samples were confirmed by standard addition methods, which was further used to investigate the practical application of the as-fabricated PEC sensor. As shown in Table 1, the recoveries showed the satisfactory results between 98.0% and 106.6%, indicating the practicality of the PEC sensor, which implied that the PEC sensor has a promising feature for detection of CAP in real samples.

4. Conclusions

In this paper, a facile method was used to prepare MoS_2/NGH hydrogels for the PEC determination of CAP. Due to π-π stacking interaction, aptamer was effectively anchored on MoS_2/NGH hydrogels without any modification. The MoS_2/NGH hydrogels could remarkably improve the PEC performance which can be ascribe to electronic interaction between NGH and MoS_2. Unlike conventional spectrophotometric methods, the PEC platform translated visible-light driven energy into remarkable photocurrent output at 0 V potential, which can greatly avoid interferences. The designed aptasensor hold the advantages of high sensitivity, good selectivity, a wide linear range and acceptable stability. In addition, the fabricated sensor had been successfully applied to detect CAP in real honey samples. The detection limits of the bioassay was 3.23 ng/L. Such MoS_2/NGH hydrogels may hold promising applications, for applications in areas including sensor, environmental monitoring, analytical and electroanalytical chemistry.

Acknowledgments

The present work was supported by the National Natural Science Foundation of China (Nos. 21675066, 21375050, 21405063 and 21505055), the Natural Science Foundation of Jiangsu province (No. BK20150486), Key Laboratory of Modern Agriculture Equipment and Technology (No. NZ201109), and a Project Funded by the Priority Academic Program Development of Jiangsu Higher Education Institutions (No. PAPD-2014-37) and Qing Lan Project.

Appendix A. Supporting information

Supplementary data associated with this article can be found in the online version at doi:10.1016/j.bios.2018.11.018.

References

Carraro, F., Calvillo, L., Cattelan, M., Favaro, M., Righetto, M., Nappini, S., Píš, I., Celorrio, V., Fermín, D.J., Martucci, A., Agnoli, S., Granozzi, G., 2015. ACS Appl. Mater. Interfaces 7, 25685–25692.
Chang, C., Zhu, L.Y., Wang, S.F., Chu, X.L., Yue, L.F., 2014. ACS Appl. Mater. Interfaces 6, 5083–5093.
Chao, Y.F., Jalili, R., Ge, Y., Wang, C.Y., Zheng, T., Shu, K.W., Wallace, G.G., 2017. Adv. Funct. Mater. 27, 1700234.
Ge, L., Wang, W.,X., Hou, T., Li, F., 2016a. Biosens. Bioelectron. 77, 220–226.
Ge, L., Wang, W.,X., Sun, X.M., Hou, T., Li, F., 2016b. Anal. Chem. 88, 2212–2219.
Gilje, S., Han, S., Wang, M.S., Wang, K.L., Kaner, R.B., 2007. Nano Lett. 7, 3394–3397.
Hao, N., Zhang, X., Zhou, Z., Qian, J., Liu, Q., Chen, S.B., Zhang, Y., Wang, K., 2017. Sens. Actuators B-Chem. 250, 476–483.
Huang, Z.Y., Han, W.J., Tang, H.L., Ren, L., Chander, D.S., Qi, X., Zhang, H., 2015. 2D Mater. 2, 035011.
Hou, T., Xu, N.N., Wang, W.X., Ge, L., Li, F., 2018. Anal. Chem. 90, 9591–9597.
Hou, Y., Wen, Z.H., Cui, S.M., Guo, X.R., Chen, J.H., 2013. Adv. Mater. 25, 6291–6297.
Hou, Y., Zhang, B., Wen, Z.H., Cui, S.M., Guo, X.R., He, Z., Chen, J.H., 2014. J. Mater. Chem. A 2, 13795–13800.
Hu, W.W., Chen, Q.S., Li, H.H., Ouyang, Q., Zhao, J.W., 2016. Biosens. Bioelectron. 80, 398–404.
Hu, X.F., Deng, F., Huang, W.Y., Zeng, G.S., Luo, X.B., Dionysiou, D.D., 2018. Chem. Eng. J. 350, 248–256.
Impens, S., Reybroeck, W., Vercammen, J., Courtheyn, D., Ooghe, S., Wasch, K.D., Smedts, W., Brabander, H.D., 2003. Anal. Chim. Acta 483, 153–163.
Jaiswal, M.K., Carrow, J.K., Gentry, J.L., Gupta, J., Altangerel, N., Scully, M., Gaharwar, A.K., 2017. Adv. Mater. 29, 1702037.
Jiang, D., Du, X.J., Chen, D.Y., Li, Y.Q., Hao, N., Qian, J., Zhong, H., You, T.Y., Wang, K., 2016a. Carbon 102, 10–17.
Jiang, D., Du, X.J., Chen, D.Y., Zhou, L., Chen, W., Li, Y.Q., Hao, N., Qian, J., Liu, Q., Wang, K., 2016b. Biosens. Bioelectron. 83, 149–155.
Jiang, D., Du, X.J., Zhou, L., Li, H.N., Wang, K., 2017. Anal. Chem. 89, 4525–4531.
Jiang, D., Liu, Q., Wang, K., Qian, J., Dong, X.Y., Yang, Z.T., Du, X.J., Qiu, B.J., 2014. Biosens. Bioelectron. 54, 273–278.
Jiang, X.Y., Zhang, L., Liu, Y.L., Yu, X.D., Liang, Y.Y., Qu, P., Zhao, W.W., Xu, J.J., Chen, H.Y., 2018. Biosens. Bioelectron. 107, 230–236.
Jiang, Y.Q., Chowdhury, S., Balasubramanian, R., 2017. Chem. Eng. J. 327, 751–763.
Jodat, A., Jodat, A., 2014. Desalin. Water Treat. 52, 2668–2677.
Li, M.J., Zheng, Y.N., Liang, W.B., Yuan, R., Chai, Y.Q., 2017. ACS Appl. Mater. Interfaces 9, 42111–42120.
Lingappan, N., Kang, D.J., 2016. Electrochim. Acta 193, 128–136.
Lin, H.P., Chen, C.C., Lee, W.W., Lai, Y.Y., Chen, J.Y., Chen, Y.Q., Fu, J.Y., 2016. RSC Adv. 6, 2323–2336.
Liu, X.Q., Huo, X.H., Liu, P.P., Tang, Y.F., Xu, J., Ju, H.X., 2017. Biosens. Bioelectron. 92, 171–178.
Liu, Y., Yan, K., Zhang, J.D., 2016. ACS Appl. Mater. Interfaces 8, 28255–28264.
Liu, Y., Yan, K., Okoth, O.K., Zhang, J.D., 2015. Biosens. Bioelectron. 74, 1016–1021.
Long, H., Trochimczyk, A.H., Pham, T., Tang, Z.Y., Shi, T.L., Zettl, A., Carraro, C., Worsley, M.A., Maboudian, R., 2016. Adv. Funct. Mater. 26, 5158–5165.
Meng, F.K., Li, J.T., Cushing, S.K., Zhi, M.J., Wu, N.Q., 2013. J. Am. Chem. Soc. 135, 10286–11028.
Miao, Y.B., Gan, N., Li, T.H., Zhang, H.R., Cao, Y.T., Jiang, Q.L., 2015. Sens. Actuators B-Chem. 220, 679–687.
Posyniak, A., Zmudzki, J., Niedzielska, J., 2003. Anal. Chim. Acta 483, 307–311.
Rodziewicz, L., Zawadzka, I., 2008. Talanta 75, 846–850.
Shi, J.P., Tong, R., Zhou, X.B., Gong, Y., Zhang, Z.P., Ji, Q.Q., Zhang, Y., Fang, Q.Y., Gu, L., Wang, X.N., Liu, Z.F., Zhang, Y.F., 2016. Adv. Mater. 28, 10664–10672.
Tao, X.Q., Jiang, H.Y., Yu, X.Z., Zhu, J.H., Wang, X., Wang, Z.H., Niu, L.L., Wu, X.P., Shen, J.Z., 2013. Drug Test. Anal. 5, 346–352.
Tian, H.W., Liu, M., Zheng, W.T., 2018. Appl. Catal. B-Environ. 225, 468–476.
Toth, P.S., Velický, M., Bissett, M.A., Slater, T.J.A., Savjani, N., Rabiu, A.K., Rakowski, A.M., Brent, J.R., Haigh, S.J., O'Brien, P., Dryfe, R.A.W., 2016. Adv. Mater. 28, 8256–8264.
Unusan, N., 2009. Int. J. Food Sci. Nutr. 60, 359–364.
Wu, S.J., Zhang, H., Shi, Z., Duan, N., Fang, C.C., Dai, S.L., Wang, Z.P., 2015. Food Control 50, 597–604.
Xu, H., Han, X.Y., Dai, X., Liu, W., Wu, J., Zhu, J.T., Kim, D.Y., Zou, G.F., Sablon, K.A., Sergeev, A., Guo, Z.X., Liu, H.Y., 2018. Adv. Mater. 30, 1706561.
Xu, Y., Cheng, C., Du, S.C., Yang, J.Y., Yu, B., Luo, J., Yin, W.Y., Li, E.P., Dong, S.R., Ye, P.D., Duan, X.F., 2016. ACS Nano 10, 4895–4919.
Zang, Y., Lei, J.P., Ju, H.X., 2017. Biosens. Bioelectron. 96, 8–16.
Zhao, W.W., Xu, J.J., Chen, H.Y., 2015. Chem. Soc. Rev. 44, 729–741.
Zhao, W.W., Xu, J.J., Chen, H.Y., 2016. TrAC-Trends Anal. Chem. 82, 307–315.
Zhao, W.W., Xu, J.J., Chen, H.Y., 2017. Biosens. Bioelectron. 92, 294–304.
Zhou, X., Hu, X.Z., Yu, J., Liu, S.Y., Shu, Z.W., Zhang, Q., Li, H.Q., Ma, Y., Xu, H., Zhai, T.Y., 2018. Adv. Funct. Mater. 28, 1706587.